

Spatial distribution of electron emission sites for sulfur doped and intrinsic nanocrystalline diamond films

F.A.M. Köck^{a,*}, J.M. Garguilo^a, R.J. Nemanich^a, S. Gupta^b, B.R. Weiner^c, G. Morell^d

^aDepartment of Physics, North Carolina State University, Raleigh, NC 27695-8202, USA

^bDepartment of Physics, University of Puerto Rico, P.O. Box 23343, San Juan, PR 00931, USA

^cDepartment of Chemistry, University of Puerto Rico, P.O. Box 23346, San Juan, PR 00931, USA

^dDepartment of Physical Sciences, University of Puerto Rico, P.O. Box 23323, San Juan, PR 00931, USA

Abstract

We have investigated high sp^2 content intrinsic and sulfur doped nanocrystalline diamond films to study field emission properties by electron emission microscopy operated in different modes. Electron emission microscopy enables real time imaging of the electron emission from a surface with a lateral resolution of ~ 15 nm. The nanocrystalline intrinsic diamond films exhibit electron emission at room temperature from localized emission sites with weak temperature dependence, and a density of $\sim 10^3$ – $10^4/\text{cm}^2$. In contrast, sulfur doped diamond films show similar emission characteristics at room temperature, but at elevated temperatures the emission significantly increases from the localized regions and a thermionic component is identified in the I/V dependence. We discuss the role of S-donor states to explain the enhanced emission of the S-doped nanocrystalline diamond.

© 2003 Elsevier Science B.V. All rights reserved.

Keywords: Nanocrystalline; Plasma CVD; Field emission

1. Introduction

High brightness, low power electron sources are the subject of ongoing interest due to their wide application range. Many carbon based materials show electron emission properties that meet the requirements for device related electron sources by exhibiting a high current density and a low threshold field with values as low as 0.5 V/ μm reported [1]. At room temperature, these films exhibit electron emission from localized sites, with the exact mechanism of the emission still unknown. Several groups have conducted extensive studies and proposed different approaches for the emission mechanism.

The localized site emission is consistent with field enhancement effects. Analysis of the current–voltage (I/V) curves would suggest enhancement factors of greater than 100 and for some samples greater than 1000. One approach for explaining this electron emission

takes into account the occurrence of conducting grain boundaries within the film [2–4]. In this model variations in conductance would result in the field enhancement. Alternatively, it has been proposed that electron emission is induced by complex nanometer scale structures at the surface [5].

To date, most measurements of electron emission have been performed at room temperature. However, at elevated temperatures changes in the electron emission characteristics can give additional insight on the electronic structure of the material.

A recent report from NC State noted the observation of a temperature dependence of the emission from N-doped diamond films [6]. Unlike the films of this study, the N-doped films exhibit poor emission characteristics at room temperature, but at temperature of 600 °C, the films are observed to exhibit emission uniformly across the surface. This result has been attributed to the role of N-dopants supplying electrons to the conduction band of the diamond or to defect bands just below the conduction band minimum.

In this study, we report detailed observations of emission from undoped nanocrystalline diamond and S-doped nanocrystalline diamond. A weak temperature

*Corresponding author. Tel.: +1-919-515-2474; fax: +1-919-515-7331.

E-mail address: fakoeck@unity.ncsu.edu (F.A.M. Köck).

dependence is observed for the emission from the intrinsic nanocrystalline diamond films, but the S-doped nanocrystalline diamond films exhibit a significant temperature dependence while the emission originates largely from localized regions on the surface. We suggest that defects and dopants incorporated into the nanocrystalline diamond give rise to electronic states that determine the electron emission properties.

2. Experimental details

The substrate material used for this study was Si $\langle 100 \rangle$, with a diameter of 25 mm and a resistivity below $1 \Omega \text{ cm}$. The surface preparation included a 30 min ultrasonic abrasion in a diamond/titanium/ethanol suspension, followed by a rinse with methanol and drying with nitrogen gas. A diamond/metal-powder based suspension results in an enhanced nucleation density compared to a diamond only suspension [7]. A 1500 W ASTeX IPX3750 microwave assisted CVD system with an RF induction heated graphite susceptor was employed for the growth of the intrinsic nanocrystalline diamond films. The process gases were zero grade N_2 , H_2 and CH_4 . During film growth laser reflectance interferometry was used for in situ monitoring of the thickness of the diamond layer. The growth conditions for the intrinsic nanocrystalline diamond films were 180 sccm H_2 , 20 sccm CH_4 , chamber pressure of 20 Torr, substrate temperature of 900°C and a microwave power of 900 W.

The sulfur doped nanocrystalline diamond films were prepared by hot filament CVD on polished Mo substrates, and the procedures are described in detail elsewhere [8].

The PEEM and field-electron emission microscopy (FEEM) measurements were completed in an Elmitec UHV-photo electron emission microscope with a base pressure of less than 1×10^{-10} Torr. The system has sample heating to $>1000^\circ\text{C}$ that was used to degas the sample surface at 150°C and to obtain temperature dependent emission measurements. The field of view can be changed from 150 to $1.5 \mu\text{m}$ with a resolution better than 15 nm. For all imaging measurements a high voltage of 20 kV is applied between the anode and the sample surface, and the anode is positioned 2–4 mm from the surface (resulting in an applied field of 10–5 V/ μm). In the FEEM measurements the emission was due to the high applied field. The electron emission current from the sample surface can be monitored and recorded to obtain current–voltage dependences. Electrons emitted from the sample pass through a perforated anode and are imaged using electron optics. The emitted electrons are intensified with a microchannel plate and imaged with a fluorescent screen. A CCD camera is used for image capturing. The images reported here

have been digitally processed to remove imperfections of the image intensifier.

In addition to FEEM measurements at various temperatures, electron emission at elevated temperatures was studied in a thermionic electron emission system, where an anode can be placed at a variable distance from the sample surface. A voltage difference of up to 5000 V can be applied between sample and anode, and the corresponding I/V characteristics can be recorded at a fixed sample anode spacing. Variable distance field emission measurements, where the anode is stepped a known distance towards the sample was employed to determine the threshold field of the films for emission at ambient temperature.

The surface morphology was studied by scanning electron microscopy (SEM) using a JEOL JSM-6400F scanning microscope.

3. Results

The focus of this study is the temperature dependence of the electron emission of the intrinsic nanocrystalline diamond and the sulfur doped nanocrystalline diamond. The films are first studied to establish the spatial dependence of the emission, and then the temperature dependence of the emission is imaged and the I/V dependence is recorded.

Both films exhibited similar threshold fields for emission as measured by the variable distance system. Threshold fields of 3.7 and $6.4 \text{ V}/\mu\text{m}$ were observed from the intrinsic and the sulfur doped nanocrystalline diamond films, respectively, for an emission current of 0.25 nA.

The nanocrystalline diamond films were first studied by electron emission microscopy in order to locate emission sites and calculate the emission site density followed by SEM investigation to determine the surface morphology. FEEM was employed to determine the emission site distribution. Fig. 1 depicts a large region of the intrinsic nanocrystalline diamond film surface imaged in FEEM mode with five clearly identified emission sites, resulting in an emission site density of approximately $5 \times 10^3/\text{cm}^2$ at an electric field of $5 \text{ V}/\mu\text{m}$. Fig. 2 displays an emission site of the S-doped film. This film also displayed an emission site density of $\sim 10^4/\text{cm}^2$. These densities are comparable to many prior reports of efficient emitting films. The lateral dimension of the emitting sites appears to be near the instrument resolution of 15 nm. Note that studies that employ a fluorescing anode to measure emission site densities cannot establish the dimensions of the emission site [9].

Intrinsic nanocrystalline diamond as well as sulfur doped diamond exhibit electron emission from localized sites as is shown in Figs. 1 and 2, respectively. However, as shown in Fig. 3, both films exhibit a uniform surface

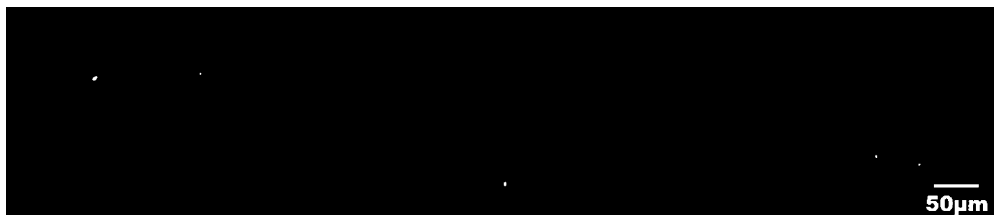


Fig. 1. FEEM of a region of intrinsic nanocrystalline diamond showing five emission sites.

morphology that indicates the presence of small grains presumably separated by conducting, sp^2 graphite containing boundaries [10]. The sulfur doped film apparently exhibits a smaller grain size than the intrinsic nanocrystalline. Grain sizes for the intrinsic film are of the order of $\sim 0.5 \mu\text{m}$ while for the sulfur doped films SEM indicates a grain dimension of $\sim 0.1 \mu\text{m}$.

The temperature dependence of a single emission site from the intrinsic nanocrystalline diamond film is displayed in Fig. 4. Increasing the sample temperature results in a very small change in the emission structure that is at the detection limit of the electron emission microscope when imaged at small field of views.

However, in Fig. 5 the thermionic I/V measurements show a distinct temperature dependence of the electron emission of the intrinsic nanocrystalline diamond. We note that the thermionic I/V measurements employ a large anode, which allows measurement of the emission from many sites. Performing a Fowler–Nordheim analysis of the data by plotting $\log I$ vs. $1/V$, it can be determined if the emission characteristic exhibits F–N behavior by fitting with a straight line. Our results indicate that the electron emission pattern is described by Fowler–Nordheim tunneling. There was no evidence of a thermionic emission component which would be observed at low electric fields, but at increased electric fields the temperature dependence becomes more pronounced.

The electron emission from individual sites in the sulfur doped nanocrystalline increases substantially as the temperature increases. A FEEM image shown in Fig. 6 displays two emission sites. In the image the central point of the brightest site was moved off the image intensifier to minimize damage to the system.

The thermionic I/V measurements shown in Fig. 7 clearly indicate a thermionic component of the emission current that can be observed at low electric fields. At low temperatures below $170 \text{ }^\circ\text{C}$, an electron emission current cannot be detected at low electric fields indicating that no significant electron tunneling occurs. Increasing the temperature at low electric fields results in a significant electron emission that can be attributed to thermally excited electrons. In addition, the I/V curves at higher electric fields display a strong contribution characteristic of a tunneling current.

4. Discussion

Two factors that influence field emission are the work function and the field enhancement. Effects of these two quantities cannot be easily separated in analysis of field emission I/V curves. Electron energy distribution measurements can provide information related to the work function, and measurements on nanocrystalline diamond have indicated that the work function of the emission sites approaches 5 eV [11]. Therefore, large field enhancement factors of greater than 100 and in some cases greater than 1000 are required to explain the observed field emission measurements. The observation of bright localized emission sites in the FEEM images in Figs. 1 and 2 is consistent with a large field enhancement.

It has been established that field emission is often inversely related to crystal quality [12]. In the case of nanocrystalline diamond we find that electron emission improves with a decline in crystal quality (i.e. increased

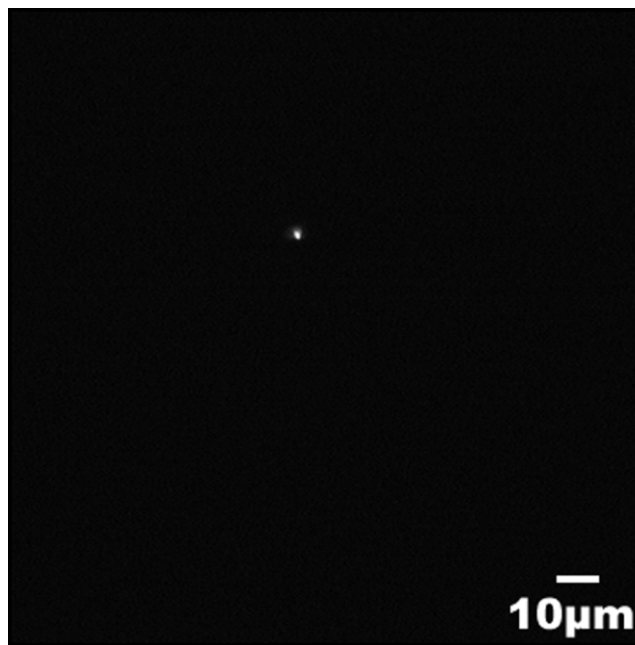


Fig. 2. FEEM of sulfur doped nanocrystalline diamond showing electron emission originating from an emission site.

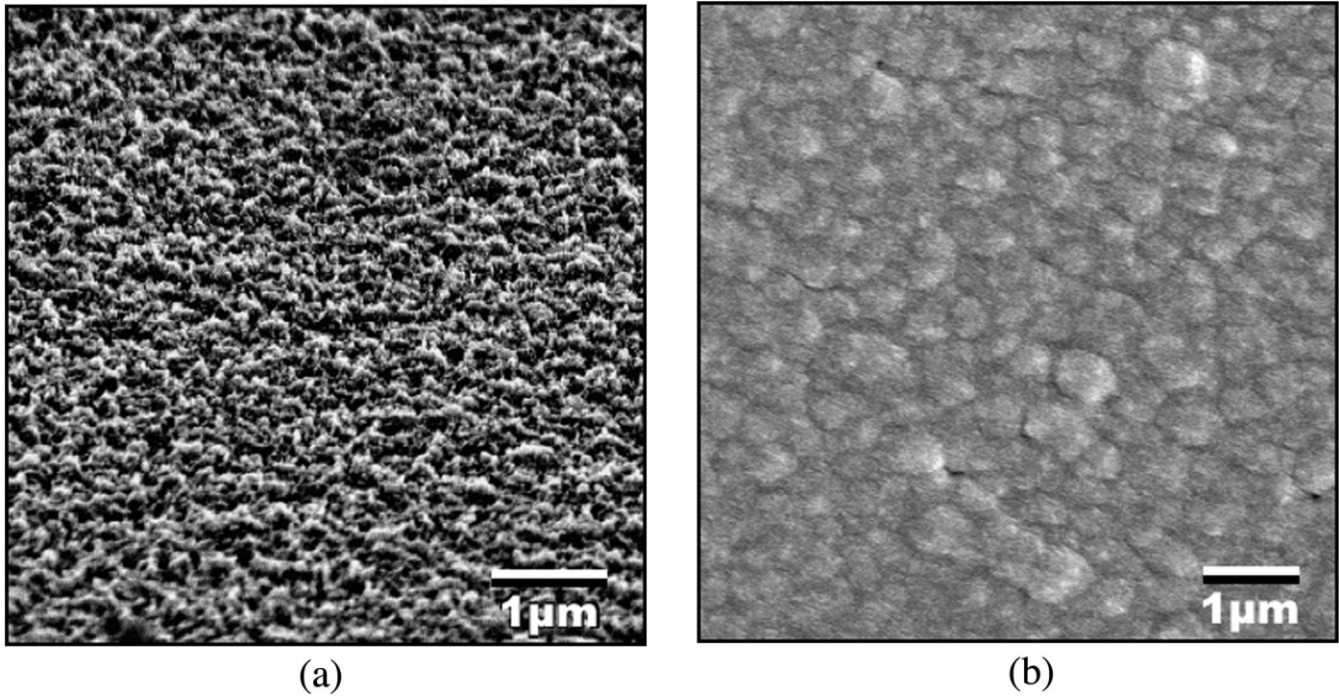


Fig. 3. SEM images of sulfur doped (left) and intrinsic (right) nanocrystalline diamond films.

sp^2 bonding and broadened diamond Raman peak), which correlates directly to an increase in defect density [13]. In undoped diamond, defects are practically the only mechanism by which electron transport can occur thus limiting the emission to sites with a favorable electronic structure [14]. Because of the large work function of the emission sites, this emission mechanism should not exhibit a strong temperature dependence consistent with our results.

The total field emission current is generated by contributions from the conduction band J_c , defect bands J_d , the valence band J_v and surface bands J_s with each of them exhibiting a particular temperature dependence.

It is well known that field emission from the valence band has negligible temperature dependence so it can be neglected. Defect induced states can significantly alter the emission characteristics if their structure allows hopping conduction within the bands or excitation from the valence band thus providing carrier transport to the surface or near surface states from which tunneling can occur. Although electron emission microscopy detects a small change in the electron emission at elevated temperatures from the individual emission site, the large area thermionic electron emission measurements show a more substantial increase (Fig. 5) that may be caused by the temperature dependence of the individual com-

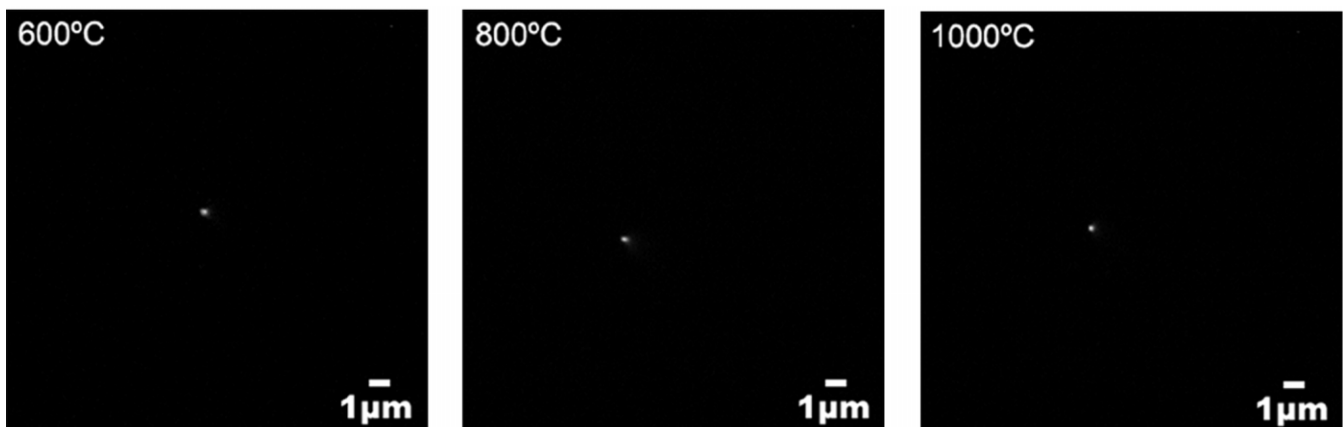


Fig. 4. T-FEEM of nanocrystalline diamond films showing no detectable increase in electron emission with an increase in temperature.

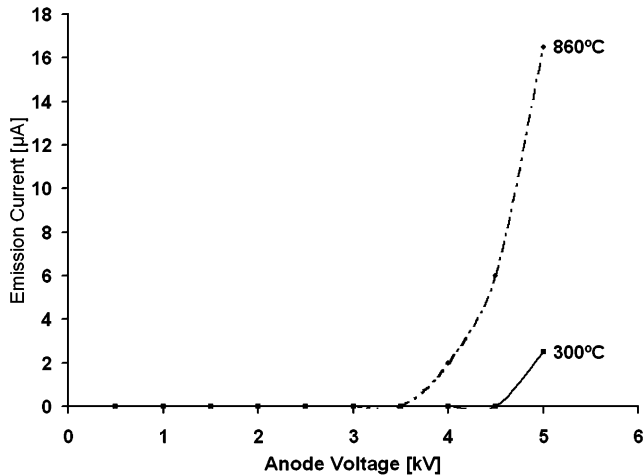


Fig. 5. Thermionic electron emission measurement of undoped nanocrystalline diamond at 300 and 860 °C with a sample-anode spacing of 2 mm.

ponents J_c , J_d and J_s . The I/V results from Fig. 5 indicate that tunneling processes prevail with a negligible thermionic component. The results indicate that as the temperature is increased carriers are promoted into near surface states from which tunneling can occur.

The abundance of grain boundaries for either film as observed by SEM in Fig. 3 cannot solely account for the bright electron emission from the few emission sites. The details of the emission mechanisms of the individual emission sites is still an important question.

N-type doping of diamond has been reported through the incorporation of sulfur. The theoretical activation energy of 0.375 eV has been observed in experimental temperature dependence plots [15,16]. Measurements on sulfur doped diamond performed by Sakaguchi et al. have furthermore shown a strong increase in the carrier concentration from approximately $10^{13}/\text{cm}^3$ at room temperature to approximately $10^{16}/\text{cm}^3$ at 300 °C with a maximum in the mobility at room temperature that moderately decreases with the relationship of $T^{-1.5}$ [17]. The temperature dependence of the concentration of ionized donors within a crystal can be described by $N_d^+ = N_d \exp(-E_a/kT)$, where N_d^+ is the ionized donor concentration and E_a is the energy level of the donor states. The shallow sulfur donor states should thus have a significant effect on field emission at elevated temperatures (Fig. 8).

The schematic band diagram in Fig. 8 shows the shallow sulfur donor states S as well as defect states D . Applying a high electric field leads to a high field enhancement factor which is indicated by the highly sloped line at the vacuum side. N-type diamond exhibits upward band bending at the surface, which is reduced due to field penetration of the applied electric field. Electron emission at low electric fields can occur from

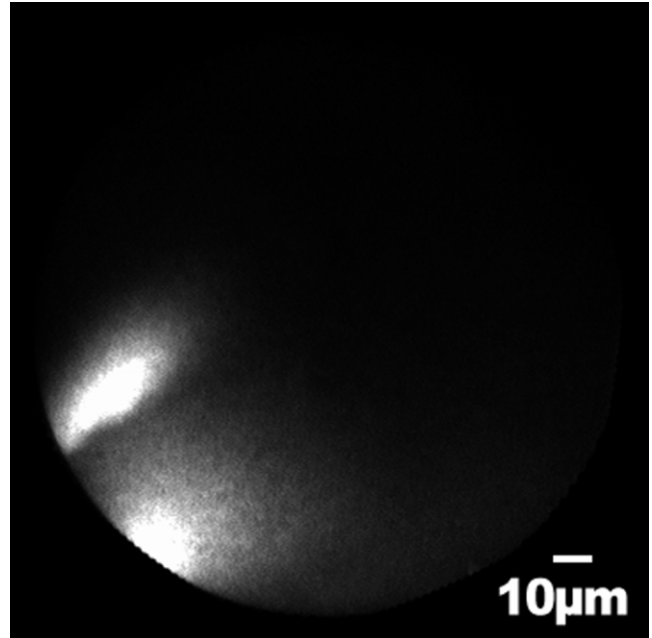


Fig. 6. T-FEEM of sulfur doped nanocrystalline diamond showing increased electron emission originating from localized regions.

thermally excited carriers from the sulfur states and at high electric fields from defect and sulfur states due to tunneling from sites with a high field enhancement factor. As shown in Fig. 2, sulfur doped nanocrystalline diamond exhibits electron emission from preferred emission sites at room temperature. Supplying thermal energy would release additional carriers that would now be emitted mainly through the existing emission sites. We can observe this behavior by studying thermionic field electron emission microscopy (T-FEEM) of the material. Fig. 6 depicts electron emission from a sulfur doped nanocrystalline diamond surface at a temperature of 340

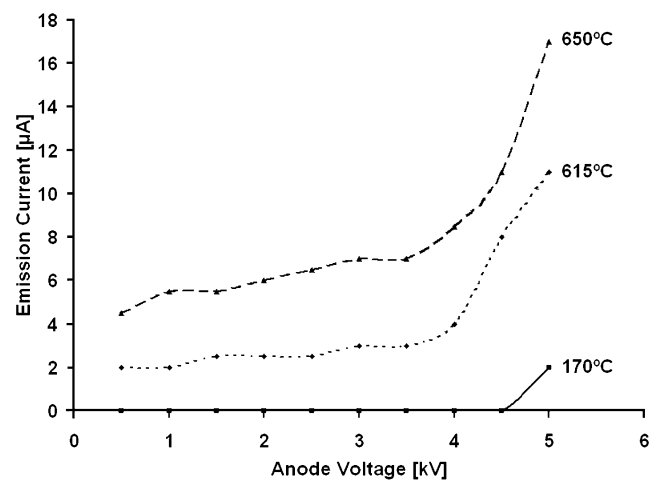


Fig. 7. Thermionic electron emission measurement of sulfur doped nanocrystalline diamond at various temperatures.

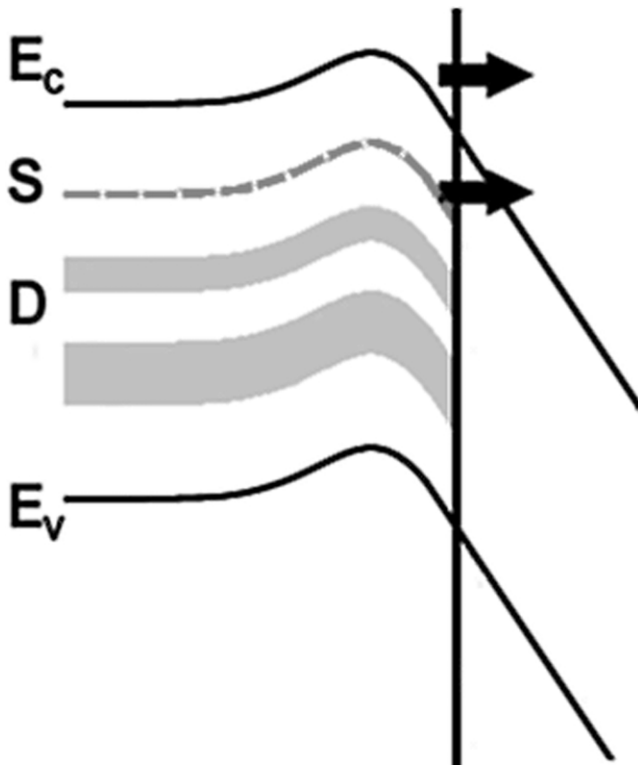


Fig. 8. Schematic band structure of sulfur doped nanocrystalline diamond showing enhanced electron emission at elevated temperatures due to the concentration increase of ionized donors S. (The location and width of the defect-induced states D are for illustration only.)

°C with a significant increase in electron emission originating from the localized regions.

The I/V curves in Fig. 7 indicate two regions for the electron emission behavior for the S-doped film. At low electric fields the electron emission does not change significantly with the applied electric field indicating a thermionic emission component, and at higher electric fields the emission is attributed to tunneling. As the temperature increases the curves are shifted indicating an increase in electron emission. Results obtained by electron emission microscopy are generally obtained at high electric fields thus imaging electrons emitted mainly due to tunneling processes.

An important question for future research will be to determine whether the thermionic and tunneling components of the emission originate from the same region of the sample. We note that our prior studies of N-doped diamond have shown a spatially uniform distribution of the thermionic emission component [6]. The S-doped materials are unusual in that they exhibit both tunneling emission sites at room temperature and an additional thermionic component at elevated temperatures.

The electronic structure of the material is a key parameter in the emission mechanism. In addition, the

temperature dependence of the electron emission indicates that donor states can significantly change the emission behavior at elevated temperatures. The results suggest that the electronic structure is not uniform throughout the film but exhibits variations that cause the observed emission characteristics.

5. Conclusions

Electron emission microscopy measurements of intrinsic and S-doped nanocrystalline diamond films indicate emission from localized regions with similar threshold fields and emission site density. The intrinsic films exhibit a small increase in electron emission from localized sites while S-doped samples display a much larger increase at elevated temperatures. The I/V measurements for undoped nanocrystalline diamond films exhibit weak temperature dependence consistent with tunneling from high work function sites. The I/V measurements of the S-doped samples show both a thermionic and tunneling contribution indicating that n-type doping plays a role in the emission. While this study has established the presence of bright emission sites in the S-doped nanocrystalline diamond, future research is necessary to establish the spatial dependence of the thermionic and tunneling components of the emission.

Acknowledgments

We gratefully acknowledge the Duke University Free Electron Laser Laboratory where all the Electron Emission Microscopy Experiments were performed. This research is supported through the Frontier Carbon Technology Project, the Japan Fine Ceramics Center, and PTS Company.

References

- [1] K. Okano, S. Koizumi, S.R.P. Silva, G.A.J. Amaratunga, *Nature* 381 (1996) 140.
- [2] J.W. Steeds, A. Gilmore, K.M. Bussmann, J.E. Butler, P. Koidl, *Diamond Relat. Mater.* 8 (1999) 996–1005.
- [3] V.D. Frolov, A.V. Karabutov, S.M. Pimenov, V.I. Konov, V.P. Ageev, *Diamond Relat. Mater.* 10 (2001) 1719–1726.
- [4] A.V. Karabutov, V.D. Frolov, S.M. Pimenov, *Diamond Relat. Mater.* 8 (1999) 763–767.
- [5] L. Nilsson, O. Groening, O. Kuettel, P. Groening, L. Schlappbach, *J. Vac. Sci. Technol. B* 20 (2002) 1023–1071.
- [6] F.A.M. Köck, J.M. Garguilo, B. Brown, R.J. Nemanich, *Diamond Relat. Mater.* 11 (2002) 774–779.
- [7] R. Shima, Y. Chakk, M. Foman, A. Hoffman, *J. Vac. Sci. Technol. B* 17 (1999) 1912–1918.
- [8] S. Gupta, B.R. Weiner, G. Morell, *Diamond Relat. Mater.* 10 (2001) 1968–1972.
- [9] J.B. Cui, J. Robertson, W.I. Milne, *J. Appl. Phys.* 89 (2001) 5707–5711.
- [10] F. Cleri, P. Keblinski, L. Colombo, D. Wolf, S.R. Phillpot, *Europhys. Lett.* 46 (5) (1999) 671–677.
- [11] O. Gröning, O.M. Küttel, P. Gröning, L. Schlappbach, *J. Vac. Sci. Technol. B* 17 (5) (1999) 1970–1986.

- [12] K.H. Park, S. Lee, K.H. Song, et al., *J. Vac. Sci. Technol. B* 16 (1998) 724–728.
- [13] S. Praver, K.W. Nugent, D.N. Jamieson, J.O. Orwa, L.A. Bursill, J.L. Peng, *Chem. Phys. Lett.* 332 (2000) 93–97.
- [14] Y. Show, F. Matsuoka, M. Hayashi, H. Ito, M. Iwase, T. Izumi, *J. Appl. Phys.* 84 (11) (1998) 6351–6354.
- [15] H. Zhou, Y. Yokoi, H. Tamura, et al., *Jpn. J. Appl. Phys.* 40 (2001) 2830–2832.
- [16] I. Sakaguchi, M.N. Gamo, Y. Kikuchi, E. Yasu, H. Haneda, *Phys. Rev. B* 60 (1999) R2139–R2141.
- [17] M.T. Kuo, P.W. May, M.N.R. Ashfold, *Diamond Relat. Mater.* 11 (2002) 1422–1428.